

# Surface Chemistry of Gold Nanoparticles Produced by Laser Ablation in Aqueous Media

Jean-Philippe Sylvestre,<sup>†</sup> Suzie Poulin,<sup>†</sup> Andrei V. Kabashin,<sup>†</sup> Edward Sacher,<sup>\*,†</sup> Michel Meunier,<sup>†</sup> and John H. T. Luong<sup>\*,‡</sup>

Laser Processing Laboratory, Department of Engineering Physics, École Polytechnique de Montréal, Case Postale 6079, succ. Centre-ville, Montréal, Québec, Canada H3C 3A7, and Biotechnology Research Institute, National Research Council Canada, Montréal, Québec, Canada H4P 2R2

Received: June 30, 2004; In Final Form: July 27, 2004

The femtosecond laser ablation of a gold target in aqueous solutions has been used to produce colloidal Au nanoparticles with controlled surface chemistry. A detailed chemical analysis showed that the nanoparticles formed were partially oxidized by the oxygen present in solution. The hydroxylation of these Au–O compounds, followed by a proton loss to give surface Au–O<sup>−</sup>, resulted in the negative charging of the nanoparticles. The partial oxidation of the gold nanoparticle surface enhances its chemical reactivity and consequently has a strong impact on its growth. In particular, the oxidized surface reacted efficiently with Cl<sup>−</sup> and OH<sup>−</sup> to augment its net surface charge. This limited the coalescence of the particles, due to electrostatic repulsion, and led to a significant reduction of their size. Taking advantage of the repulsion effect, efficient size control was achieved using different salts (7 ± 5 nm for 10 mM KCl, 5.5 ± 4 nm for 10 mM NaCl, 8 ± 5 nm for NaOH, pH 9.4), a considerable improvement comparatively to particles prepared in deionized water, using identical ablation conditions, where particles of 1–250 nm were produced. The partially oxidized gold surface was also suitable for surface modification through both covalent and electrostatic interactions during particle formation. Using solutions of *N*-propylamine, we showed an efficient control of nanoparticle size (5–8 ± 4–7 nm) by the involvement of these interactions. The results obtained help to develop methodologies for the control of laser-ablation-based nanoparticle growth and the functionalization of nanoparticle surfaces by specific interactions.

## Introduction

The laser ablation of a solid target immersed in a liquid milieu has become an increasingly important “top down” method for fabricating nanostructured materials.<sup>1–41</sup> This physical approach was originally used to produce noble metal nanoparticles with “bare” surfaces, which cannot be achieved with wet chemical methods.<sup>1–7</sup> Indeed, wet chemical procedures, such as, for example, the reduction of a precursor salt with a reducing agent, often lead to surface contamination, mainly by residual anions and the reducing agent.<sup>3–7,42</sup> On the other hand, laser ablation in liquids is expected to result in various chemical reactions between the ablated species and molecules in the liquid, because the ejected species are highly excited, both electronically and translationally.<sup>43</sup> While chemical reactions and crystalline phase transformations are observed for chemically reactive materials (Al, Cu, Ni, Si, Ti, graphite, etc.),<sup>3,8–15,18–20,33,35</sup> the ablation of noble metals, such as gold and silver, in solvents, such as water, ethanol, and *n*-hexane,<sup>37</sup> results mainly in metallic particles. In chloroform as the liquid environment, gold and silver react with the chlorine.<sup>37</sup> To our knowledge, the surface chemistry of gold nanoparticles fabricated by laser ablation in aqueous media has not previously been thoroughly investigated.

An understanding of the surface chemistry of the gold particles is of importance, since most of their intended applications require further functionalization of their surfaces.<sup>44</sup> For

example, small gold nanoparticles (<30 nm), exhibiting a surface plasmon resonance peak at 520 nm, may be exploited for various biosensing and biotechnological applications. Such applications require the attachment of a ligand to the particle surface to provide the selective and specific binding of a target analyte. The size control of the noble metal nanoparticles fabricated by laser ablation could be achieved by adding specific molecules to the aqueous fabrication environment, which physically or chemically interact with the surfaces of the forming particles, to limit their growth. Ionic surfactants,<sup>17,24–27</sup> cyclodextrins,<sup>39,40</sup> and sodium chloride<sup>5–7,36</sup> were successfully used to limit the noble metal particle size. In some cases, the exact mechanism limiting the growth of the particles remains unclear.

In this study, we investigate the surface composition of the gold particles produced by laser ablation in deionized water. We also explore the effect of various compounds, such as salts and amines, to elucidate the role of surface modification in the size control of the particles obtained. This is a first step toward the application of such surface-functionalized nanoparticles.

## Experimental Section

Laser ablation was carried out with a Ti/sapphire laser (Hurricane, Spectra Physics Lasers), which provided 120 fs full width at half-maximum (fwhm) pulses (wavelength 800 nm, maximum energy 1 mJ/pulse, repetition rate 1 kHz, beam diameter 7 mm). The beam was expanded to 21 mm diameter before being focused by an objective, with a focal length of 7.5 cm, onto a gold rod with a diameter of 6 mm (99.99%, Alfa Aesar). The gold target was placed on the bottom of a 3 mL glass vessel filled with an aqueous solution. The surface of

\* To whom correspondence should be addressed. E-mail: edward.sacher@polymtl.ca (E.S.); john.luong@nrc-nrc.gc.ca (J.H.T.L.).

<sup>†</sup> École Polytechnique de Montréal.

<sup>‡</sup> National Research Council Canada.

the gold rod was polished before each experiment. The depth of the deionized water layer above the target was 12 mm. The vessel was placed on a horizontal platform that revolved at a constant speed of 0.5 mm/s. Typically, the focal plane was adjusted 1.5 mm beyond the target surface to decrease the radiation intensity on its surface and enlarge the radiation spot. This weakened the plasma intensity and thus minimized the impact of plasma-related ablation effects that were found to broaden the size distribution of the ablated nanoparticles.<sup>41</sup> Under such conditions, the rate of particle formation is estimated to be 0.01 mg/min of ablation. The laser energy was fixed at 0.2 mJ/pulse during all experiments unless otherwise specified.

All aqueous solutions used as ablation environments were prepared from deionized water (18 M $\Omega$  cm). NaCl (99+%), KCl (99+%), NaNO<sub>3</sub> (99+%), HCl (0.1 N solution in water), NaOH (0.1 N solution in water), and *n*-propylamine (99+%) were purchased from Sigma-Aldrich and used as received. Dialysis of the Au colloids was used to eliminate unbonded materials, and was carried out on a 6000–8000 MW dialysis membrane immersed in a 4 L container filled with deionized water. The time of dialysis was at least 24 h, and the water was changed every 6 h.

X-ray photoelectron spectroscopy (XPS) took place in a VG ESCALAB 3 Mark II, using a nonmonochromated Mg K $\alpha$  X-ray source at 1253.6 eV, and a base pressure below 10<sup>-10</sup> Torr. For sample preparation, drops of the colloidal solution were placed on freshly cleaved highly oriented pyrolytic graphite (HOPG) substrates, and dried overnight in a pumped desiccator. High-resolution spectra were obtained at a perpendicular takeoff angle, using a pass energy of 20 eV and steps of 0.05 eV. Spectral peaks were separated using the VG Advantage program, and a Shirley background was subtracted. The energy was calibrated by setting the major C1s HOPG peak to 284.5 eV.

FTIR spectra, with a resolution of 4 cm<sup>-1</sup>, were obtained with an Excalibur Series spectrometer, FTS3000 (Bio-Rad Laboratories). Drops of the solution to be analyzed were placed on a ZnSe (Irtran-4) substrate and dried overnight, in a pumped desiccator, prior to measurement. Time-of-flight static secondary ion mass spectroscopy (TOF-SIMS) took place in an ION-TOF TOF-SIMS IV. An isotopic <sup>69</sup>Ga<sup>+</sup> source was used in the high-current bunch mode to obtain a mass resolution of >8000 on <sup>29</sup>Si. The beam voltage was 25 kV, with a target current of 1.5 pA and 27.5 ns pulses. Several drops of nanoparticles prepared in deionized water were placed on a Si substrate and dried overnight in a pumped desiccator.

$\zeta$  potential measurements were performed with the Zetasizer ZS (Malvern). Typically, 100  $\mu$ L of the gold solution was added to 900  $\mu$ L of the same solution used for the fabrication of the particles, and the resulting diluted gold sol was injected into the electrophoretic cell. Absorption spectra of the colloidal solutions were obtained immediately after production, in the spectral region 350–800 nm, with a Lambda 19 UV–vis spectrometer (Perkin-Elmer). A transmission electron microscope (TEM Philips CM30), with 0.23 nm point-to-point resolution, was used to obtain micrographs of the gold nanoparticles. Samples were prepared by placing a drop of solution on a carbon-coated, Formvar-covered copper grid, and dried at room temperature.

## Results

**Ablation in Deionized Water.** To develop possible strategies for the size and surface chemistry control of gold nanoparticles prepared by laser ablation in aqueous media, we first examined the properties of gold colloids prepared in deionized water.

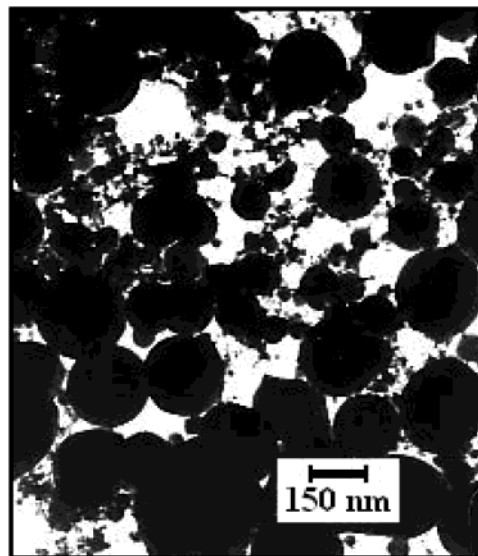


**Figure 1.** TEM micrograph image of gold particles prepared by the femtosecond laser ablation of gold in deionized water.

Figure 1 shows that the size of the nanoparticles produced was strongly dispersed. Although most nanoparticles were relatively small (15–40 nm), some were significantly larger with diameters to 200–250 nm. As we showed in our previous study,<sup>41</sup> size distributions with such a strong dispersion can be fit by a superposition of two Gaussian functions (narrow and broad distributions). The appearance of these distributions was attributed to the contributions of the radiation- and plasma-related mechanisms to the ablation. Details on the analysis of nanoparticle size distributions in deionized water, and mechanisms of material ablation, can be found elsewhere.<sup>41</sup> Under our conditions, the maximum of the first radiation-related distribution was around 20 nm, whereas the maximum of the broad, plasma-related one was around 70 nm. We note that the relative contribution of the plasma-related mechanism can be weakened or undetected by a decrease of laser energy during the experiment,<sup>41</sup> leading to a reduction of the mean size of the nanoparticles produced in deionized water. The energy decrease is accompanied by a decrease in the efficiency of nanoparticle production. In this study, the energy we used, 0.2 mJ/pulse, was a compromise between the relatively small nanoparticle size and the relatively high production efficiency. Despite a relatively strong dispersion of the nanoparticles produced, they exhibited a peak in the absorption spectrum, associated with the excitation of surface plasmons (Figure 2). Basically, 3–30 nm nanoparticles are known to show the plasmon-related peak around 520 nm. Under our experimental conditions, this peak was around 550 nm and slightly broadened, consistent with a larger size and higher nanoparticle dispersion.

XPS studies illustrated that the particles produced were partially oxidized. A high-resolution spectrum of the Au4f core level, shown in Figure 3, can be characterized by three pairs of peaks due to Au4f<sub>7/2</sub> and Au4f<sub>5/2</sub> spin–orbit coupling. While the positions of the first and most important pair (BEs of 84 and 87.3 eV) are related to elemental gold (Au<sup>0</sup>), those of the other pairs are related to the only two stable gold oxide states, Au<sup>+</sup> (BEs of 85.6 and 89.1 eV) and Au<sup>3+</sup> (BEs of 87.3 and 90.4 eV). On the basis of relative peak areas, their respective atomic percentages were estimated as 88.7% for Au<sup>0</sup>, 6.6% for Au<sup>+</sup>, and 4.7% for Au<sup>3+</sup>.

FTIR spectra of gold nanoparticles exhibited a broad peak in the region 3000–3600 cm<sup>-1</sup>, which is attributed to OH

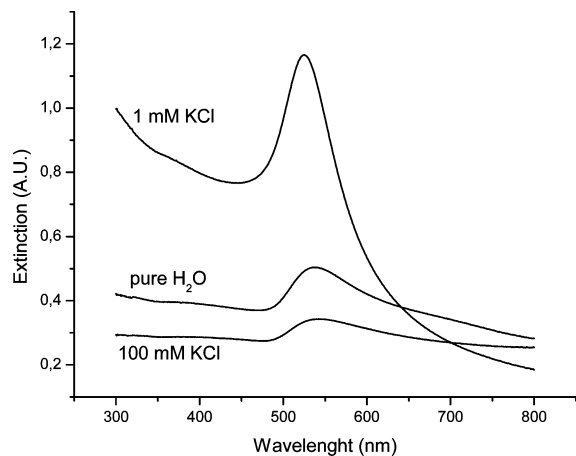


**Figure 2.** Absorption spectra of gold colloids produced by laser ablation in different aqueous solutions.

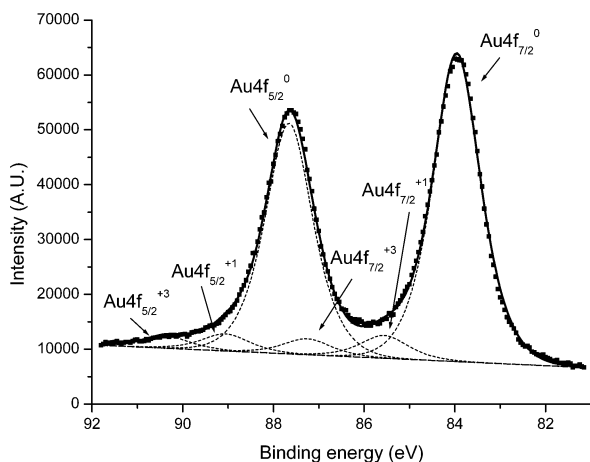


**Figure 3.** High-resolution Au4f XPS spectrum of Au nanoparticles produced by laser ablation in deionized water.

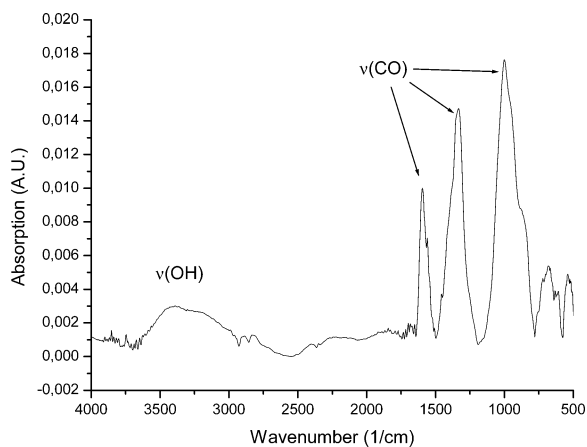


**Figure 4.** FT-IR spectra of gold nanoparticles produced in deionized water.

stretching (Figure 4). The other three peaks, centered at 1000, 1334, and 1595  $\text{cm}^{-1}$ , are assigned to the stretching modes of carbonato ( $\text{CO}_3$ ) complexes coordinated to a metal.<sup>45</sup> The presence of these chemical groups on the gold particle surface indicates the presence of Au–O compounds.

Negative TOF-S-SIMS spectra of the Au nanoparticles (Figure 5) revealed the presence of  $\text{Au}^-$  (197.96 amu),  $\text{AuO}^-$  (212.95 amu),  $\text{AuOH}^-$  (213.96 amu),  $\text{CO}_3\text{Au}^-$  (256.93 amu), and  $\text{CHO}_3\text{Au}^-$  (257.94 amu). This is a confirmation of the XPS and FTIR results, and gives direct evidence that gold nanopar-

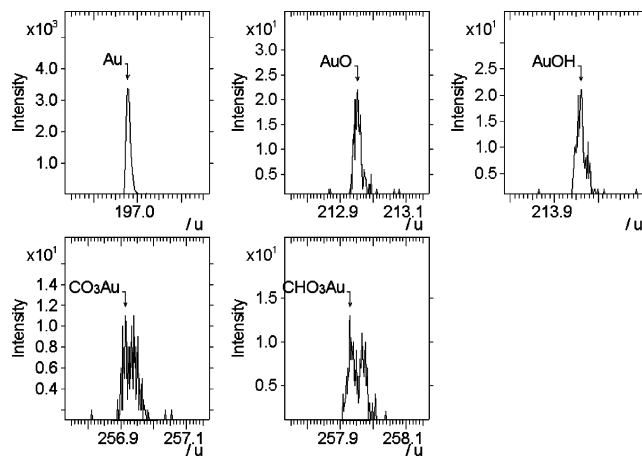


**Figure 5.** Negative TOF-S-SIMS spectra for mass regions corresponding to  $\text{Au}^-$ ,  $\text{AuO}^-$ ,  $\text{AuOH}^-$ ,  $\text{CO}_3\text{Au}^-$ , and  $\text{CHO}_3\text{Au}^-$ . Particles were prepared in deionized water.

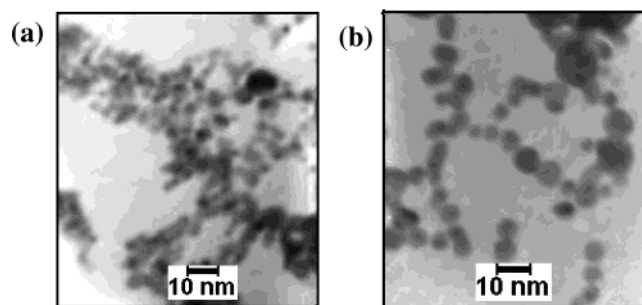


**Figure 6.** TEM micrographs of gold particles prepared by the femtosecond laser ablation of gold in (a) 10 mM NaCl and (b) NaOH (pH 9.4).

ticles are partially oxidized, with OH and  $\text{CO}_3$  groups present on the gold surface. The information obtained on the partial gold oxidation modifies our view of potential nanoparticle reactivity and reveals novel possibilities for chemical manipulation with the gold nanoparticle surface.

**Ablation in Ionic Solutions.** On the basis of the surface chemistry of the Au nanoparticles produced in deionized water, we carried out studies on gold surface modifications, through the introduction of potentially reactive chemical groups into the water environment. Laser ablation was carried in KCl, NaCl, HCl, NaOH, and  $\text{NaNO}_3$ . First, we studied the colors of the solutions after fabrication, and their corresponding absorption spectra. It is known<sup>24–27</sup> that the color of the colloidal solution (and its absorption spectrum) is a good indicator of the particle size and solution stability against aggregation, as a consequence of the size-dependent properties of surface plasmons. In addition, we measured the size of the nanoparticles by TEM.

The presence of KCl, NaCl, and NaOH had a similar effect on the colors of the colloids obtained. At relatively low concentrations of these chemicals (below  $\leq 10$  mM), the sols were pink or bright red. The absorption spectra for all three solutions were characterized by the presence of a sharp plasmon-related peak at 520 nm. An example of the absorption spectrum for 1 mM KCl is given in Figure 2. The plasmon-related peak was much narrower and stronger compared to that of particles prepared in deionized water, suggesting the production of much smaller particles. This was confirmed by TEM analysis. Figure 6 shows typical TEM micrographs of nanoparticles produced in both NaOH, pH 9.4, and 10 mM NaCl. The nanoparticles were relatively small and only slightly dispersed. Furthermore, in contrast to that of the nanoparticles produced by femtosecond

**TABLE 1: Particle Size Distributions Obtained in Different Aqueous Media**

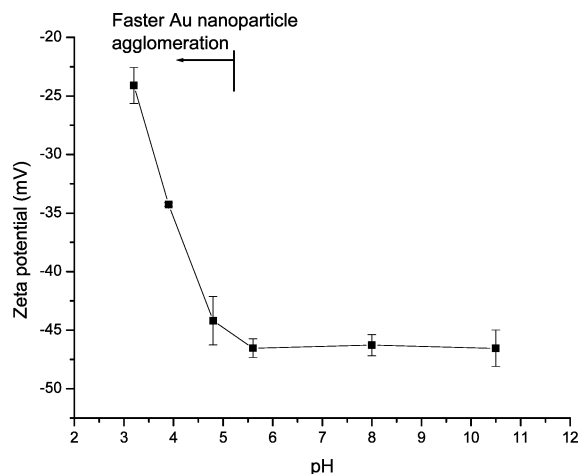
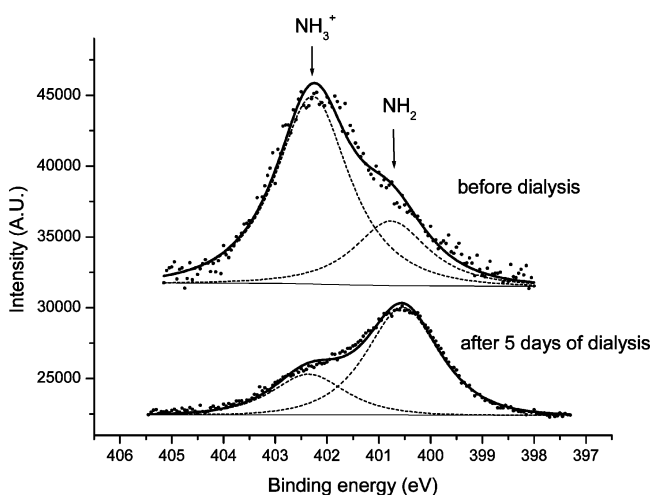
aqueous medium	laser energy (mJ/pulse)	size distribution (nm)	mean particle size (nm)
deionized water	0.2	1–250	40
10 mM NaCl	0.2	1–12	5.5
10 mM KCl	0.2	1–15	7
NaOH, pH 9.4	0.2	1–18	8
10 mM propylamine	0.25	1–16	7

ablation in deionized water,<sup>41</sup> the size distribution of the nanoparticles produced in KCl, NaCl, and NaOH can be fit by a single Gaussian distribution, indicating that the simple addition of a salt controlled the growth of nanoparticles ablated by both radiation- and plasma-related mechanisms. In other words, the population of the larger particles present in deionized water, for identical ablation conditions, is quenched by the presence of a salt. It should be noted that this is no longer the case when a very high laser fluence is used. The mean size and dispersion of the nanoparticles, estimated from TEM images, were 5.5 and 4 nm fwhm, respectively, for 10 mM NaCl, 7 and 5 nm fwhm for 10 mM KCl, and 8 and 5 nm fwhm for NaOH, pH 9.4. Table 1 summarizes the particle size distributions obtained in different aqueous solutions.

However, at higher concentrations of KCl, NaCl, and NaOH (>10 mM), we observed quite different colloidal solution properties. In these cases, the solutions were blue with a gray tint, a color usually associated with the agglomeration of nanoparticles. Further, the Au particles began to precipitate within a few hours. As shown in Figure 2, the absorption spectrum of nanoparticles produced at 100 mM KCl was characterized by a much weaker plasmon-related peak, shifted to 540–550 nm, suggesting both relatively large nanoparticle sizes and size dispersions. This was confirmed by TEM analysis indicating the absence of any reduction effect compared to that of pure deionized water. A similar decrease or absence of the reduction effect was observed in experiments with HCl (pH < 5.8) and NaNO<sub>3</sub>. In these cases, the sols were blue with a gray tint, and the particles completely precipitated within hours, independent of the salt concentration, while the absorption spectra were similar to those obtained in 100 mM KCl (Figure 2).

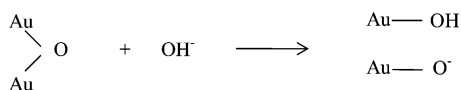
These results for the different salts indicate that OH<sup>-</sup> and Cl<sup>-</sup> interact with the Au surface during particle formation. The effect of Cl<sup>-</sup> is, however, negligible in acid solutions, as indicated by results obtained for HCl. To clarify the effect of the OH<sup>-</sup> concentration, we measured the  $\zeta$  potential of gold particles produced in 10 mM NaCl at different pH values (adjusted with HCl or NaOH). The particles produced were negatively charged for all samples in the pH range explored. As shown in Figure 7, the absolute value of the  $\zeta$  potential below pH 5.8 decreased as the pH decreased whereas, above pH 5.8, the absolute value of the  $\zeta$  potential became almost constant. The  $\zeta$  potential is of the same order of magnitude, with a reported value of -35 mV for 20 nm diameter citrate-stabilized colloidal gold particles.<sup>46</sup> The experiments below pH 5.8 were accompanied by a much faster agglomeration of the gold colloids. This process was especially pronounced at pH 3, where agglomeration occurred during particle fabrication. Faster agglomeration is consistent with the measured decrease of the surface charge, leading to a reduction of the electrostatic repulsion between negatively charged nanoparticles.

The measurement of the  $\zeta$  potential of the particles as a function of pH confirms the presence of hydroxyl groups on the Au particle surface. Indeed, hydroxyl groups (-OH) are in

**Figure 7.**  $\zeta$  potential of gold nanoparticles produced in 10 mM aqueous NaCl solutions at different pH values.**Figure 8.** High-resolution XPS spectra of the nitrogen (N1s) peak of gold nanoparticles produced by laser ablation in a 10 mM aqueous solution of propylamine. The upper figure is an as-produced sample, while the lower one was dialyzed for 5 days prior to measurement.

equilibrium with -O<sup>-</sup>, and their relative abundance is dictated by the pH value of their environment relative to the pK value of the hydroxylated surface. When the pH is below the pK value, -OH is dominant, and when the pH is above the pK value, -O<sup>-</sup> is dominant. Under our experimental conditions, the oxidized portion of the gold surface should almost exclusively have Au-O<sup>-</sup> groups at pH > 5.8 and increasing numbers of Au-OH groups at pH < 5.8.

**Ablation in *N*-Propylamine.** We also verified that *n*-propylamine interacts with the Au surface. *N*-Propylamine was specifically selected as a model study to investigate interactions between nanoscale Au colloids and the amine group. Ablation (250 mJ/pulse) in 10 mM *n*-propylamine resulted in bright red gold sols after several minutes, indicating the formation of small gold particles. The sols were also stable for several months when stored in capped bottles, at room temperature. TEM measurements (not shown) confirmed that particles with a mean size of 5–8 nm and a dispersion of less than 4–7 nm were produced. To better understand the nature of the interaction, XPS studies were carried out. A high-resolution Au4f spectrum was obtained (not shown) and was almost identical to the one obtained for gold in pure water (Figure 3). High-resolution N1s spectra were also obtained for samples as-prepared (Figure 8, top) and after being dialyzed for 5 days to eliminate unbonded *n*-propylamine (Figure 8, bottom). The experimental spectra were separated

**SCHEME 1: Conversion of Surface Oxide to Hydroxide**

into two peaks, one at about 402.3 eV, attributed to ammonium ion ( $-\text{NH}_3^+$ ), and another at about 400.6 eV, attributed to amine ( $-\text{NH}_2$ ). Notice that the ammonium ion is dominant in the undialyzed sample, while the amine dominates after dialysis. This is a strong indication that the unprotonated *n*-propylamine is chemisorbed to the gold particle surface while the ammonium ion interacts electrostatically with the negatively charged nanoparticles. These electrostatic interactions are sufficiently strong for the protonated *n*-propylamine to remain bound to the gold even under the high-vacuum conditions of XPS, but cannot withstand extensive dialysis.

**Discussion**

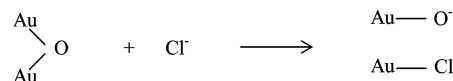
Our studies revealed that nanoparticles, produced by laser ablation in deionized water, are not exclusively formed of metallic  $\text{Au}^0$  as widely expected, but also contain  $\text{Au}^+$  and  $\text{Au}^{3+}$ . These oxidation states of gold are mainly due to  $\text{Au}-\text{O}$  compounds, as such products were found on the gold nanoparticle surface by both FTIR and TOF-S-SIMS. These compounds probably result from chemical reactions between highly excited ejected Au atoms (or ions) or clusters and oxygen-containing species present in the laser-generated plasma or at the plasma/water interface. The presence of carbonate complexes on the gold nanoparticles ( $\text{Au}-\text{OCO}_2^-$  and  $\text{Au}-\text{OCO}_2\text{H}$ ) also revealed by both FTIR and TOF-S-SIMS is probably due to the presence of atmospheric  $\text{CO}_2$ . It is not yet clear, however, if the reaction of  $\text{CO}_2$  with the gold surface occurs partly in solution ( $\text{CO}_2$  is slightly soluble in water, forming trace amounts of  $\text{HCO}_3^-$  and  $\text{H}^+$ ) or when the dried sample, prepared for analysis, is exposed to air.

On the basis of  $\zeta$  potential measurements, the pH-dependent ionization of the oxidized particles contributes to the negative charge carried by the gold nanoparticles. Such a model has already been used to explain the pH dependence of the negatively charged surfaces of gold films<sup>47</sup> and nanoparticles.<sup>42</sup> An increase in the hydroxyl concentration favors the conversion of the surface oxide to hydroxide, as shown in Scheme 1. This is supported by the fact that gold colloids prepared by dispersion through ultrasonic agitation of an evaporated gold thin film in water required preconditioning in NaOH, pH 9.5, to obtain negatively charged nanoparticles.<sup>42</sup>

The absolute surface charge of the gold nanoparticles, which increases with pH, may have a determining role on the size control of the particles produced and may explain the reason nanoparticles prepared in NaOH solutions were smaller than those produced in deionized water. The highly negatively charged nanoparticles produced in basic solution will tend to repel each other, thus limiting particle coalescence.

Compared to those produced by ablation in deionized water, the gold particles produced in NaCl and KCl were smaller for identical laser fluences. Similar results were obtained for the production of silver nanoparticles prepared by the nanosecond laser ablation of a silver target immersed in aqueous NaCl solutions.<sup>5-7,36</sup> This was attributed to the relatively high affinity of the chloride anions for the silver surface.<sup>6</sup>

Unlike nitrate,<sup>42</sup> chloride ion is known to display a relatively high affinity for gold. Therefore, NaCl and KCl exhibit size-reducing effects, but  $\text{NaNO}_3$  does not. However, the effect of chloride ions is still unclear since ablation in HCl (pH < 5.8)

**SCHEME 2: Surface Dissociation of Gold Oxide Compounds Favored by the Presence of Chloride Ions**

was not found to have a size-reducing effect. We reason that the size reduction effect of chloride is related to the surface charge of the nanoparticles. The chloride ion has a tendency to react with  $\text{Au}-\text{O}$  compounds, as shown in Scheme 2, transferring its negative charge to the particle. When the pH is above 5.8, the  $\text{Au}-\text{O}^-$  formed remains intact and contributes to the overall negative charge. Below this pH, with HCl, most of the  $\text{Au}-\text{O}^-$  sites become  $\text{Au}-\text{OH}$ , and the resulting surface has a smaller net charge, with no size-reducing effect on the nanoparticles.

High concentrations of NaOH, NaCl, and KCl result in unstable colloids, and such behavior was also observed for silver nanoparticles prepared in NaCl.<sup>36</sup> This may seem surprising, as lower concentrations of the same salts resulted in stable sols. In fact, this may be explained in terms of the electrical double layer thickness. A charged surface placed in an electrolyte will attract counterions to form the electrical double layer; its thickness decreases as the concentration of the electrolyte increases.<sup>48</sup> When the electrical double layer thickness becomes too small, the surface charges on the gold nanoparticles are screened out, and the long-range electrostatic repulsions are no longer effective. This phenomenon is commonly called the salting-out effect.<sup>48</sup>

Ablation in *n*-propylamine also results in nanoparticles smaller than those obtained in deionized water. Our XPS study revealed that both amine ( $-\text{NH}_2$ ) and ammonium ion ( $-\text{NH}_3^+$ ) are present. Extensive dialysis of the colloids results in the elimination of most of the ammonium ion. We reason that the  $-\text{NH}_2$  is covalently bound to the gold nanoparticles while the  $-\text{NH}_3^+$  is electrostatically bound to the negatively charged gold surface, explaining the dialysis results. In general, amines do not react with bulk Au; however, nanosized Au sols do react with amine groups<sup>49,50</sup> to form a "weak covalent bond".<sup>49</sup> Those sols are, however, prepared by the reduction of  $\text{HAuCl}_4$ , a fabrication method known to leave residual contaminants (chloride, reducing agent) on a negatively charged particle, thus raising the possibility that the amine group may have reacted with a surface contaminant<sup>49</sup> rather than with the Au, per se. With laser ablation, the surface termination of the nanoparticles by *n*-propylamine, through both chemical and electrostatic interactions, is the rationale behind the size reduction effect of *n*-propylamine. Most importantly, the surface modification of gold nanoparticles during laser ablation in amine-containing liquids can be envisaged for the functionalization of Au nanoparticles. It is expected that thiol-containing molecules could similarly be used to control particle size and surface chemistry during laser ablation in liquid, as the covalent interaction between thiols and Au nanoparticles has been extensively investigated in the literature.<sup>51-54</sup> Experiments are now under way to verify this.

While all the colloids studied here were fabricated using femtosecond laser radiation, we anticipate that similar results are to be expected with nanosecond laser ablation in aqueous media. It should be noted that nanosecond lasers also ablate excited species that may potentially react with molecules present in the surrounding liquid. A femtosecond laser, with higher intensity and lower energy, forms smaller nanoparticles than does a nanosecond laser.<sup>39-41</sup> Nevertheless, an exact mechanism

of the formation of nanoparticles, provoked by femtosecond laser ablation, remains to be elucidated.

## Conclusions

The nanoparticles obtained by laser ablation were partly oxidized, with Au–O compounds present at the nanoparticle surface. These compounds contribute to the negative surface charge of the nanoparticles. The addition of  $\text{Cl}^-$  or  $\text{OH}^-$  to the solution increases the absolute value of this negative charge and leads to the formation of smaller nanoparticles. In the presence of *n*-propylamine, the amine reacts with the nanoparticle surface. This is accompanied by the reduction of the particle size and is a strong indication that the simultaneous functionalization of Au nanoparticles can be achieved during their fabrication by laser ablation.

**Acknowledgment.** We thank the Natural Sciences and Engineering Research Council of Canada for funding, and Dr. D.-Q. Yang (École Polytechnique) for XPS measurements.

## References and Notes

- (1) Fojtik, A.; Henglein, A. *Ber. Bunsen-Ges. Phys. Chem.* **1993**, *97*, 252.
- (2) Henglein, A. *J. Phys. Chem.* **1993**, *97*, 5457.
- (3) Nedderson, J.; Chumanov, G.; Cotton, T. M. *Appl. Spectrosc.* **1993**, *47*, 1959.
- (4) Sibbald, M. S.; Chumanov, G.; Cotton, T. M. *J. Phys. Chem.* **1996**, *100*, 4672.
- (5) Prochazka, M.; Stepanek, J.; Vlckova, B.; Srnova, I.; Maly, P. *J. Mol. Struct.* **1997**, *410–411*, 213.
- (6) Prochazka, M.; Mojzes, P.; Stepanek, J.; Vlckova, B.; Turpin, P.-Y. *Anal. Chem.* **1997**, *69*, 5103.
- (7) Srnova, I.; Prochazka, M.; Vlckova, B.; Stepanek, J.; Maly, P. *Langmuir* **1998**, *14*, 4666.
- (8) Yang, G.-W.; Wang, J.-B.; Liu, Q.-X. *J. Phys.: Condens. Matter* **1998**, *10*, 7923.
- (9) Wang, J.-B.; Yang, G.-W. *J. Phys.: Condens. Matter* **1999**, *11*, 7089.
- (10) Yang, G. W.; Wang, J. B. *Appl. Phys. A* **2000**, *71*, 343.
- (11) Yang, G. W.; Wang, J. B. *Appl. Phys. A* **2001**, *72*, 475.
- (12) Wang, J. B.; Zhang, C. Y.; Zhong, X. L.; Yang, G. W. *Chem. Phys. Lett.* **2002**, *361*, 86.
- (13) Wang, J. B.; Yang, G. W.; Zhang, C. Y.; Zhong, X. L.; Ren, Z. H. *A. Chem. Phys. Lett.* **2003**, *367*, 10.
- (14) Liu, Q. X.; Yang, G. W.; Zhang, J. X. *Chem. Phys. Lett.* **2003**, *373*, 57.
- (15) Liu, Q. X.; Wang, C. X.; Zhang, W.; Yang, G. W. *Chem. Phys. Lett.* **2003**, *382*, 1.
- (16) Jeon, J.-S.; Yeh, C.-S. *J. Chin. Chem. Soc.* **1998**, *45*, 721.
- (17) Chen, Y.-H.; Yeh, C. S. *Colloids Surf., A* **2002**, *197*, 133.
- (18) Yeh, M.-S.; Yang, Y.-S.; Lee, Y.-P.; Lee, H.-F.; Yeh, Y.-H.; Yeh, C.-S. *J. Phys. Chem. B* **1999**, *103*, 6851.
- (19) Lee, Y.-P.; Liu, Y.-H.; Yeh, C.-S. *Phys. Chem. Chem. Phys.* **1999**, *1*, 4681.
- (20) Kao, H.-M.; Wu, R.-R.; Chen, T.-T.; Chen, Y.-H.; Yeh, C.-S. *Mater. Chem.* **2000**, *10*, 2802.
- (21) Wu, K. T.; Yao, Y. D.; Wang, C. R. C.; Chen, P. F.; Yeh, E. T. J. *Appl. Phys.* **1999**, *85*, 5959.
- (22) Hwang, C.-B.; Fu, Y.-S.; Lu, Y.-L.; Jang, S.-W.; Chou, P.-T.; Wang, C. R. C.; Yu, S. J. *J. Catal.* **2000**, *195*, 336.
- (23) Chen, C.-D.; Yeh, Y.-T.; Wang, C. R. C. *J. Phys. Chem. Solids* **2001**, *62*, 1587.
- (24) Mafuné, F.; Kohno, J.-Y.; Takeda, Y.; Kondow, T.; Sawabe, H. *J. Phys. Chem. B* **2000**, *104*, 8333.
- (25) Mafuné, F.; Kohno, J.-Y.; Takeda, Y.; Kondow, T.; Sawabe, H. *J. Phys. Chem. B* **2000**, *104*, 9111.
- (26) Mafuné, F.; Kohno, J.-Y.; Takeda, Y.; Kondow, T. *J. Phys. Chem. B* **2001**, *105*, 5114.
- (27) Mafuné, F.; Kohno, J.-Y.; Takeda, Y.; Kondow, T. *J. Phys. Chem. B* **2003**, *107*, 4218.
- (28) Tsuji, T.; Iryo, K.; Ohta, H.; Nishimura, Y. *Jpn. J. Appl. Phys.* **2000**, *39*, L931.
- (29) Tsuji, T.; Iryo, K.; Nishimura, Y.; Tsuji, M. *J. Photochem. Photobiol., A* **2001**, *145*, 201.
- (30) Tsuji, T.; Iryo, K.; Watanabe, N.; Tsuji, M. *Appl. Surf. Sci.* **2002**, *202*, 80.
- (31) Tsuji, T.; Kakita, T.; Tsuji, M. *Appl. Surf. Sci.* **2003**, *206*, 314.
- (32) Simakin, A. V.; Voronov, V. V.; Shafeev, G. A.; Brayner, R.; Bozon-Verduraz, F. *Chem. Phys. Lett.* **2001**, *348*, 182.
- (33) Dolgaev, S. I.; Simakin, A. V.; Voronov, V. V.; Shafeev, G. A.; Bozon-Verduraz, F. *Appl. Surf. Sci.* **2002**, *186*, 546.
- (34) Anikin, K. V.; Melnik, N. N.; Simakin, A. V.; Shafeev, G. A.; Voronov, V. V.; Vitukhnovsky, A. G. *Chem. Phys. Lett.* **2002**, *366*, 357.
- (35) Liu, C. H.; Peng, W.; Sheng, L. M. *Carbon* **2001**, *39*, 137.
- (36) Bae, C. H.; Nam, S. H.; Park, S. M. *Appl. Surf. Sci.* **2002**, *197–198*, 628.
- (37) Compagnini, G.; Scalisi, A. A.; Puglisi, O. *Phys. Chem. Chem. Phys.* **2002**, *4*, 2787.
- (38) Compagnini, G.; Scalisi, A. A.; Puglisi, O. *J. Appl. Phys.* **2003**, *94*, 7874.
- (39) Kabashin, A. V.; Meunier, M.; Kingston, C.; Luong, J. H. T. *J. Phys. Chem. B* **2003**, *107*, 4527.
- (40) Sylvestre, J.-P.; Kabashin, A. V.; Sacher, E.; Meunier, M.; Luong, J. H. T. *J. Am. Chem. Soc.* **2004**, *126*, 7176.
- (41) Kabashin, A. V.; Meunier, M. *J. Appl. Phys.* **2003**, *94*, 7941.
- (42) Thompson, D. W.; Collins, I. R. *J. Colloid Interface Sci.* **1992**, *152*, 197.
- (43) Sakka, T.; Iwanaga, S.; Ogata, Y. H.; Matsunawa, A.; Takemoto, T. *J. Chem. Phys.* **2000**, *112*, 8645.
- (44) Warner, M. G.; Hutchison, J. E. In *Synthesis, Functionalization and Surface Treatment of Nanoparticles*; Baraton, M.-I., Ed.; American Scientific Publishers: Stevenson Ranch, CA, 2003; pp 67–89.
- (45) Nakamoto, K. *Infrared and Raman spectra of inorganic and coordination compounds*, 4th ed.; John Wiley & Sons: New York, 1986.
- (46) Schmitt, J.; Machtle, P.; Eck, D.; Mohwald, H.; Helm, C. A. *Langmuir* **1999**, *15*, 3256.
- (47) Duval, J.; Huijs, G. K.; Throels, W. F.; Lyklema J.; van Leeuwen, H. P. *J. Colloid Interface Sci.* **2003**, *260*, 95.
- (48) Evans, D. F.; Wennerström, H. *The Colloidal Domain where Physics, Chemistry, Biology, and Technology Meet*, 2nd ed.; Wiley-VCH: New York, 1999.
- (49) Leff, D. V.; Brandt, L.; Heath, J. R. *Langmuir* **1996**, *12*, 4723.
- (50) Kumar, A.; Mandal, S.; Selvakannan, P. R.; Pasricha, R.; Mandale, A. B.; Sastry, M. *Langmuir* **2003**, *19*, 6277.
- (51) Hayatt, M. A. *Colloidal Gold: Principles, Methods, and Applications*; Academic Press: San Diego, CA, 1989.
- (52) Freeman, R. G.; Grabar, K. C.; Allsion, K. J.; Bright, R. M.; Davis, J. A.; Guthrie, A. P.; Hommer, M. B.; Jackson, M. A.; Smith, P. C.; Walter, D. G.; Natan, M. *J. Science* **1995**, *267*, 1629.
- (53) Mann, S.; Shenton, W.; Li, M.; Connolly, S.; Fitzmaurice, D. *Adv. Mater.* **2000**, *12*, 147.
- (54) Brust, M.; Bethell, D.; Schiffrin, D. J.; Kiely, C. J. *Adv. Mater.* **1995**, *7*, 795.